Journal of Materials Chemistry A

COMMUNICATION

View Article Online
View Journal | View Issue

Check for updates

Cite this: J. Mater. Chem. A, 2017, 5, 8255

Received 2nd March 2017
Accepted 12th April 2017

DOI: 10.1039/c7ta01921a

rsc.li/materials-a

Published on 12 April 2017. Downloaded by Zhejiang University on 21/06/2017 06:44:38.

Continuous fabrication of the graphene-confined polypyrrole film for cycling stable supercapacitors†

Tieqi Huang, Shengying Cai, Hao Chen, Yanqiu Jiang, Siyao Wang and Chao Gao *

A meter-length, graphene-confined polypyrrole (GP) film was fabricated by a scalable wet-spinning technology. The GP film-assembled supercapacitors had an extremely high cycling stability (115% retention after 50 000 cycles) due to the delicate graphene-confined polypyrrole-layered structures. Highly flexible supercapacitors with different sizes were further assembled with a gel electrolyte.

Polypyrrole, a typical conductive polymer, has widely been used as a pseudocapacitor for its high theoretical specific capacitance (C_S > 600 F g^{-1}) and facile preparation.[1,2] However, the performance of polypyrrole-assembled supercapacitors (PASs) sharply degrades during cycling retaining only 50% of its capacitance after 1000 charge and discharge cycles,[3] which is far below the satisfactory level of practicable supercapacitors. The cycling instability of PASs is mainly due to the volumetric deformation and counterion drain effect.[4] First, as the backbone of polypyrrole repeatedly swells and shrinks due to the movement of counterions during cycling, the structure of polypyrrole is pulverized, and the corresponding capacitance declines.[5,6] Moreover, ion channels collapse when ions diffuse back to the electrolyte, resulting in difficulty to re-dope polypyrrole into polarons and hence decreasing the conductivity and capacitance. This is called the counterion drain effect.[7] Considerable efforts have been made to improve polypyrrole cycling stability, including combining them with flexible carbon substrates such as graphene[8] and carbon nanotubes[9] and introducing doping chelating agents such as Tiron[10] and sulfanilic acid azochromotrop.[11] The cycling stability of polypyrrole-based supercapacitors is still not sufficient (*i.e.*, most cases are 1000 cycles with a record 10 000 cycles). Therefore, a fundamental strategy is needed to highly improve the cycling performance of polypyrrole-based supercapacitors.

MOE Key Laboratory of Macromolecular Synthesis and Functionalization, Department of Polymer Science and Engineering, Key Laboratory of Adsorption and Separation Materials & Technologies of Zhejiang Province, Zhejiang University, 38 Zheda Road, Hangzhou 310027, P. R. China. E-mail: chaogao@zju.edu.cn

† Electronic supplementary information (ESI) available. See DOI: 10.1039/c7ta01921a

Herein, we report a facile method to prepare a graphene-confined polypyrrole (GP) film with a greatly improved cycling stability. The pyrrole monomer was added into a suitable amount of graphene oxide, and the mixture was wet-spun into the solution containing Fe^{3+}, which was both the coagulating agent and polymerization oxidant. Taking advantage of the wet-spinning technology,[12–17] we successfully fabricated meter-length GP films. We adjusted the ratio of graphene oxide and the pyrrole component, to modify the microstructure, and optimized the performance of the assembled supercapacitors. The GP film assembled supercapacitors delivered a C_s of 302 F g^{-1} at a current density of 1 A g^{-1} with excellent rate performance (80% retention at 100 A g^{-1}). Significantly, the resulting supercapacitors showed a record cycling stability, and no decrease in capacitance was found even after 50 000 charge and discharge cycles. We attributed this outstanding performance to the delicate microstructure design of the graphene-confined polypyrrole structure formed during the wet-spinning assembly.

The fabrication step of GP film is illustrated in Fig. 1a. The wet-spinning technology for GO liquid crystals has been set up by our group previously.[18–23] We found that the solution of GO and pyrrole still displayed vivid schlieren texture by polarized-light optical microscopy (POM), which demonstrated well-preserved liquid crystals (Fig. S1†).[24–27] This means that the pyrrole monomer was dispersed well between graphene oxide sheets. The mixture of GO and pyrrole was wet-spun into the coagulation bath and then *in situ* polymerization of pyrrole occurred with Fe^{3+} as the oxidant.[28] All the composites of GO and pyrrole showed suitable solubility with different mixture weight ratios and could be continuously wet-spun into films. The wet-spinning speed of the film reached 200 m h^{-1}, which was much more efficient than the traditional preparation methods of the composites of graphene and polypyrrole (*e.g.* filtration,[29] template assist,[30] electrochemical deposition[31] and hydrothermal treatment[32]). Chemically reduced RGO gave rise to a three dimensional conductive network of hydrogel. After drying, the composite hydrogel compressed and turned into thin a GP film.

Published on 12 April 2017. Downloaded by Zhejiang University on 21/06/2017 06:44:38.

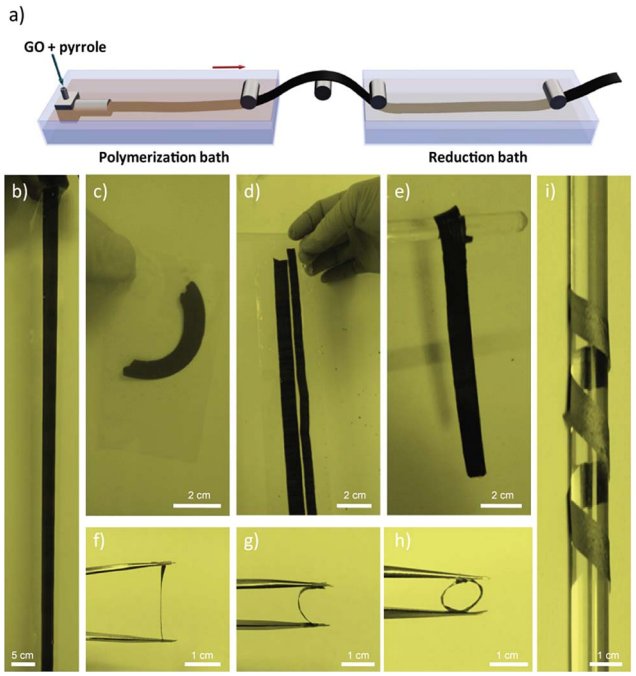

Fig. 1 (a) Schematic of the wet-spinning process of GP. (b) 1 meter-long GOP film. (c) Ring-shaped GOP film. (d) Simultaneous continuous preparation of two GOP films of different widths. (e) Free-standing GOP film without substrate. (f–h) Different bending state of GP film. (i) GP film twisted around a glass rod.

The one meter wet-spun GP film was easily fabricated as shown in Fig. 1b. Similar to the pure wet-spun GO film previously reported,[20] our GO–polypyrrole (GOP) film could also be continuously wet-spun, demonstrating that the *in situ* formed polypyrrole macromolecules did not destroy the continuity and integrity of the hydrogel. The hydrogel film could be wet-spun into not only a straight rectangular shape, but also arc or fan shape films by a wedge nozzle (Fig. 1c). A nozzle that was designed with two channels could be employed to simultaneously produce two continuous GOP films with different widths. Fig. 1d shows the preparation of 1 cm and 0.5 cm width films fabricated with the two-channel nozzle. This indicates that we can simultaneously prepare several strips with different widths by simply increasing the channels, which is in favor of industrial fabrication of GOP films. The strength of the GOP hydrogel was good enough to be free-standing without the substrate, as shown in Fig. 1e. The reduced GP film can be distorted from a straight line into a circle, demonstrating its excellent flexibility (Fig. 1f–h). We twisted the GP film around a glass rod without breakage, which indicates the high strength and toughness of the film (Fig. 1i). This outstanding flexibility may be attributed to the continuous network and the tight interaction between graphene and polypyrrole.[29,33]

The ratio of GO to pyrrole was proven to be an important factor for the electrochemical performance.[34] In order to access the best property of supercapacitors for GP-based supercapacitors (GP-S), we prepared different films with different weight ratios of GO to pyrrole. According to thermal gravimetric analysis (TGA), the corresponding weight ratios of polypyrrole in GP1, GP2, GP3, GP5 were around 49, 35, 27 and 21%, respectively (Fig. S2†). The cross-section morphology images of the GP films with different feed ratios were collected using a scanning electron microscope (SEM) in Fig. 2. The thickness of the film increased from 2 to 5 μm due to the growth of polypyrrole macromolecules. As the polypyrrole amount increased due to the increase of pyrrole monomer, the GP films remained as a layered structure with no phase separation or agglomeration, indicating good compatibility of pyrrole and graphene oxide. The uniform coverage of polypyrrole on the graphene sheets was analyzed by atomic force microscopy (AFM), and the image showed the polypyrrole bulges on the graphene sheets (Fig. 2k),[24–26,35,36] while there were only graphene wrinkles on the surface of pure RGO (Fig. S3†). The thickness of the GP2 sheet was about 3 nm (Fig. 2l), which was much higher than that of RGO (about 1.1 nm). The interlayer space was calculated by X-ray diffraction (XRD) tests, as shown in Fig. S4.† The (002) peak of the RGO film was at 25.7° (interlayer of 3.4 nm), while it was 24.7° (interlayer of 3.54 nm) for the GP2 film, which can be attributed to the intercalated polypyrrole among graphene sheets. The tensile strength of GP2 film was 90 MPa, lower than 154 MPa obtained for the RGO film (Fig. S5†). The weakened mechanical property is due to the destruction of the stacking layered structure with the interlayered polypyrrole macromolecules.

The electrochemical performance of RGO, GP5, GP3, GP2 and GP1 assembled supercapacitors (G-S, GP5-S, GP3-S, GP2-S, GP1-S) is summarized in Fig. 3a, calculated by galvanostatic charge and discharge (GCD) measurements. Among all the tested samples, the C_s of GP2-S showed the best performance of 302 F g^{-1} at 1 A g^{-1} and 243 F g^{-1} even at 100 A g^{-1}. The rate capability of GP2-S reached 80% when the current density increased 100-fold, which is on the top level of graphene–polypyrrole supercapacitors reported previously (Table S1†). When the density of GP2 reached as high as 1.7 g cm^{-3}, the specific volumetric capacitance (C_{sv}, 513 F cm^{-3}) was one among the best results reported in previous literatures (Table S2†).[37–43] We attributed the good electrochemical performance of GP2-S to the appropriate polypyrrole amount, which provided high

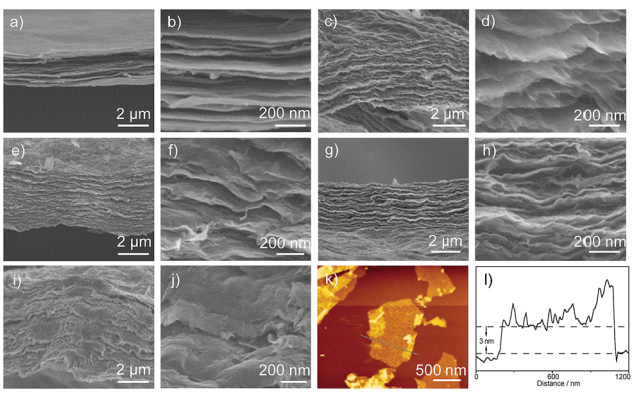

Fig. 2 Cross-sectional morphology of (a and b) RGO; (c and d) GP5; (e and f) GP3; (g and h) GP2 and (i and j) GP1. (k and l) Representative AFM image of GP2 individual sheets and its height profile.

This journal is © The Royal Society of Chemistry 2017

Published on 12 April 2017. Downloaded by Zhejiang University on 21/06/2017 06:44:38.

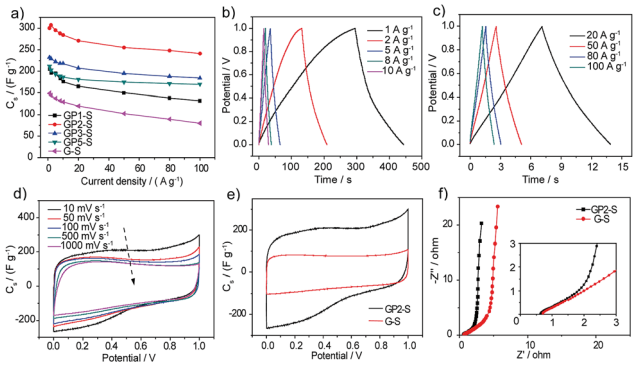

Fig. 3 Electrochemical performance of GP-Ss and G-S. (a) The rate performance of GP-Ss and G-S calculated by GCD tests; (b) GCD tests for GP2-S at different current densities from 1 to 10 A g^{-1}; (c) GCD tests for GP2-S at different current densities from 20 to 100 A g^{-1}; (d) CV tests of GP2-S at different scan rates from 10 to 1000 mV s^{-1}; (e) CV tests of GP2-S and G-S at a scan rate of 10 mV s^{-1}; (f) Nyquist plots of GP2-S and G-S, the inset shows the high frequency behavior.

pseudocapacitance without decreasing the electroconductivity too much, considering the conductivity of polypyrrole is much lower than that of graphene.[44,45] The GCD curves of GP2-S under different current densities are showed in Fig. 3d and e. Whether under low current density (1–10 A g^{-1}) or high current density (20–100 A g^{-1}), the curves of GP2-S exhibited a semi-triangular shape with distorted lines due to the pseudocapacitance.[46–48] The cyclic voltammetry (CV) curves of GP2-S from 10 to 1000 mV s^{-1} are shown in Fig. 3d. Unlike several other conductive polymer–graphene systems[49,50] or metal oxide–graphene systems,[51,52] our GP2-S still maintained a quasi-rectangular shape even if the scan rate increased to 1000 mV s^{-1}, demonstrating outstanding capacitive behaviour under high scan rates. Compared with G-S, which displayed a rectangular shape due to the double layer electrochemical property, our GP2-S showed a distorted rectangular shape with a larger area due to the pseudocapacitance derived from polypyrrole (Fig. 3e).[53] Moreover, Ragone plots further demonstrated the best performance of GP2-S, which delivered an energy density of 8.4 W h kg^{-1} at an ultrahigh average power density of 25 kW kg^{-1} (Fig. S6†). Electrochemical impedance spectroscopy (EIS) was carried out on GP2-S and G-S films to investigate their resistances from 0.1 to 100 kHz (Fig. 3f). The equivalent circuit that was used to fit the Nyquist plots is shown in Fig. S7.† The low frequency portions in Nyquist plots of GP2-S and G-S were nearly vertical to the axis of the real component, indicating ideal EDLC behaviour.[54] However, they differed from each other at high frequencies. As a part of the curve (slope of 1) named as Warburg-type line illustrates the ion diffusion and transport process,[55] GP2-S showed superior ion diffusion ability because of the suitable amount of pseudocapacitance and wrinkled porous conductive network for good connection with electrolyte ions. These electrochemical properties resulted in good pseudocapacitive behaviour and fast electrochemical responsivity.

The cycling performance of GP2-S was tested by GCD at 5 A g^{-1} for 50 000 cycles (Fig. 4a). For the first few hundred cycles, the C_s increased because the film was gradually activated, and the inner wrinkled structure was adjusted for the electrolyte ions.[56,57] After 10 000 cycles, the C_s tended to be stable around 1.15 times the initial cycle. The inset in Fig. 4a shows the GCD curves of GP2-S at 5 A g^{-1} before and after 50 000 cycles. After cycling, the GCD curve of GP2-S showed a much more obvious contorted line, indicating that the cycling process activated the electrodes to display much more pseudocapacitance delivered by polypyrrole. Significantly, the outstanding cycling stability greatly surpassed those of the reported supercapacitors based on graphene–polypyrrole systems (Fig. 4b).[29,32,58–63] This unprecedented stability can be explained by the SEM images of the film after cycling 50 000 times. In Fig. 4c and d, the general morphology was similar to the original film mentioned in Fig. 2g, which indicated that the wrinkled porous structure and three dimensional conductive network was still maintained after such a long time of cycling. Fig. S8† showed the EDS mapping analysis for the GP2 film cross section before and after cycling. Both of them showed uniform distribution of N element on the graphene sheets. Moreover, we carried out X-ray

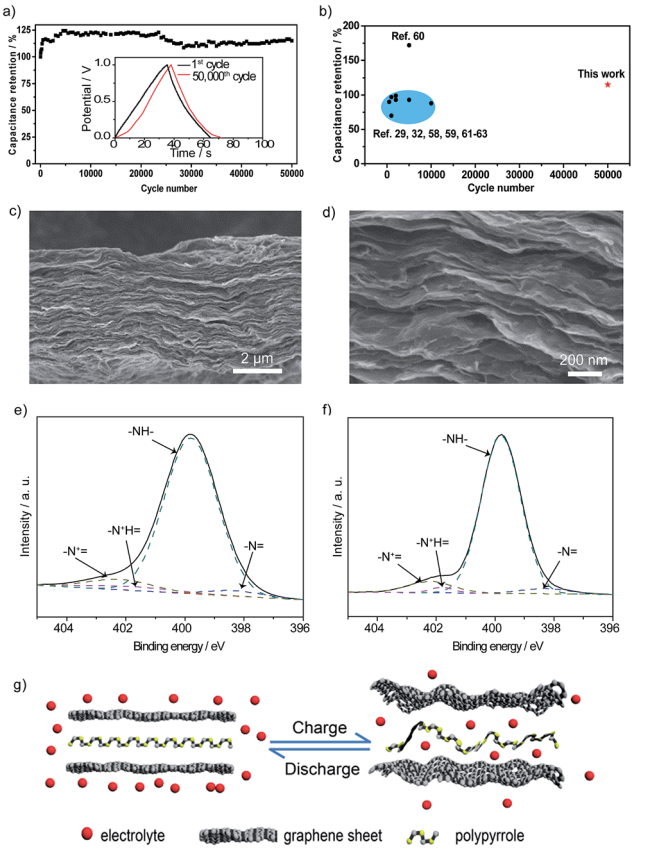

Fig. 4 (a) Cycling stability of GP2-S after 50 000 cycles at the current density of 5 A g^{-1}, the inset shows the GCD curves of GP2-S at the first and 50 000th cycle; (b) the cycling stability of GP2-S with other reported values for comparison; (c and d) SEM images of GP2 after 50 000 GCD cycles with different magnifications; (e and f) high-resolution N 1s XPS spectra of GP2 at the first and 50 000th cycle, respectively; (g) the schematic of proposed charge–discharge mechanism of GP2.

Published on 12 April 2017. Downloaded by Zhejiang University on 21/06/2017 06:44:38.

photoelectron spectroscopy (XPS) analysis to determine whether the chemical composition had changed. Fig. 4e and f show the N 1s before and after cycling, respectively. The nitrogen content of the film after 50 000 cycles (5.71%) was nearly equal to the nitrogen content of the original film (5.47%). The synthetic Gaussian peaks of the N 1s core level spectra can be assigned to nitrogen atoms (–N= at 398.3 eV, –NH– at 399.8 eV) and polarons (–N^+H– at 401.8 eV, –N^+= at 402.2 eV).[4] Since polypyrrole polarons have been extremely important to the conductivity and could be reduced to –N=,[64] the retention of polypyrrole polarons was crucial to the electrochemical performance. For GP2, the polaron ratio, defined as the content ratio of the polaron signals (–N^+H– and –N^+=) to the total nitrogen signals (–N=, –NH–, –N^+H–, –N^+=),[4] only changed from 10.6% (before cycling) to 9.7% (after cycling), illustrating that the polarons barely changed. Therefore, no apparent changes occurred in content and composition of nitrogen element during cycling. Accordingly, the stable inner structure determined the stable cyclic performance.

We assumed the possible reason for such a stable structure shown in Fig. 4g. In the conventional electrode system without the confinement of graphene layers, the polypyrrole was easy to be pulverized during cycling because of the repeated swelling and shrinking of the polymer backbones induced by the movement of ions.[5,6] In addition, the content of polarons severely decreased due to the counterion drain effect, which led to the rapid decrease in conductivity and hence the capacitance.[7] Therefore, the cycling performance of conventional polypyrrole-based supercapacitors is poor. In contrast, for our wet-spun GOP films, the pyrrole monomers inserted into the interlayers between GO sheets and the *in situ* polymerization occurred in a constrained space. As a result, the charge–discharge volumetric deformation could be accommodated by the flexible nature of graphene sheets, and the channels of polypyrrole for transmission of ions would not be collapsed due to the restricted interspace between graphene sheets. Hence, the volumetric deformation and counterion drain effect of polypyrrole can both be largely restricted by the graphene-confined structures.[4] Therefore, our GP-S exhibited outstanding cycling stability.

As free-standing films, our GP2 films can be assembled well into flexible and bendable supercapacitors. Based on continuous wet-spinning technology, we can fabricate different flexible supercapacitors with different sizes. Fig. 5a displays GP2 films-assembled flexible supercapacitors (GP2-FS) from small sizes (1 cm × 1 cm) to large sizes (2 cm × 15 cm), indicating that our GP2-FS can be processed into desirable scales and shapes. According to Fig. 5b, the GP2-FS showed quasi-rectangles as the scan rate increased from 10 to 100 mV s^{-1}, which demonstrated that our GP2-FS performed well even in the gel electrolyte with low ionic conductivity. Fig. 5c shows the charge and discharge curves from 1 to 5 mA cm^{-2}. The crooked line indicated the existence of pseudocapacitance under the gel system. We calculated the specific area capacitance (C_{ss}) and summarized them in Fig. 5d. GP2-FS showed 185 mF cm^{-2} (6.42 mW h cm^{-2}, Fig. S9†) at 1 mA cm^{-2}, and it retained 76% (140 mF cm^{-2}, 4.86 mW h cm^{-2}) when the current density increased

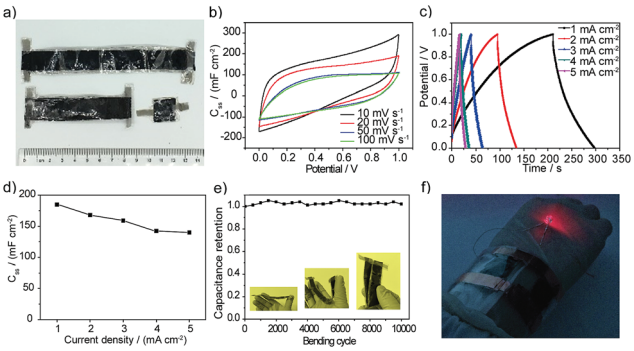

Fig. 5 The performance of GP2-FS: (a) photographs of GP2-FS of different sizes; (b) CV tests for GP2-FS at different scan rates from 10 to 100 mV s^{-1}; (c) GCD tests for GP2-FS at different current densities from 1 to 5 mA cm^{-2}; (d) the rate performance of GP2-FS calculated by GCD tests; (e) the bending stability tests, the inset shows different bending states from 0° to 180°; (f) LED lighted by the wrist strap assembled from three GP2-FS in series.

to 5 mA cm^{-2}, which was comparable to one of the best flexible supercapacitors (Table S3†). We also tested the performance of GP2-FS at the bending state (Fig. 5e). The inserted three images in Fig. 5e show the bending state from 0° to 180°. C_{ss} remained nearly unchanged even after 10 000 bending cycles, which demonstrates good flexibility and stability of our GP2-FS. We connected three GP2-FS in series and assembled them into a wrist strap, powering a light emitting diode (LED) for 2 minutes (Fig. 5f).

Conclusions

In summary, we fabricated meter-length graphene-confined polypyrrole films with scalable wet-spinning technology. The assembled supercapacitors showed high specific capacitance, good rate capability and decent flexibility. The novel, well-designed graphene-confined layered microstructures restricted the pulverization and counterion drain effect of polypyrrole, resulting in excellent cycling stability (115% retention after 50 000 cycles), which is highly favourable for practical applications of supercapacitors. The efficient and facile wet-spinning approach for the fabrication of graphene-confined, polypyrrole films may enable the industrial preparation of wearable and stable flexible supercapacitors.

Acknowledgements

This study is supported by National Key R&D Program of China (No. 2016YFA0200200), and the National Natural Science Foundation of China (No. 21325417 and No. 51533008).

References

1 S. Machida, S. Miyata and A. Techagumpuch, *Synth. Met.*, 1989, **31**, 311–318.
2 G. A. Snook, P. Kao and A. S. Best, *J. Power Sources*, 2011, **196**, 1–12.

 This journal is © The Royal Society of Chemistry 2017

Published on 12 April 2017. Downloaded by Zhejiang University on 21/06/2017 06:44:38.

3 T. Liu, L. Finn, M. Yu, H. Wang, T. Zhai, X. Lu, Y. Tong and Y. Li, *Nano Lett.*, 2014, **14**, 2522–2527.
4 Y. Song, T.-Y. Liu, X.-X. Xu, D.-Y. Feng, Y. Li and X.-X. Liu, *Adv. Funct. Mater.*, 2015, **25**, 4626–4632.
5 M. R. Gandhi, P. Murray, G. M. Spinks and G. G. Wallace, *Synth. Met.*, 1995, **73**, 247–256.
6 T. F. Otero and I. Boyano, *J. Phys. Chem. B*, 2003, **107**, 6730–6738.
7 J. Heinze, B. A. Frontana-Uribe and S. Ludwigs, *Chem. Rev.*, 2010, **110**, 4724–4771.
8 Y. Song, J.-L. Xu and X.-X. Liu, *J. Power Sources*, 2014, **249**, 48–58.
9 H. Fu, Z.-J. Du, W. Zou, H.-Q. Li and C. Zhang, *J. Mater. Chem. A*, 2013, **1**, 14943–14950.
10 K. Shi and I. Zhitomirsky, *J. Power Sources*, 2013, **240**, 42–49.
11 S. Chen and I. Zhitomirsky, *J. Power Sources*, 2013, **243**, 865–871.
12 Y. Meng, Y. Zhao, C. Hu, H. Cheng, Y. Hu, Z. Zhang, G. Shi and L. Qu, *Adv. Mater.*, 2013, **25**, 2326–2331.
13 T. Huang, B. Zheng, L. Kou, K. Gopalsamy, Z. Xu, C. Gao, Y. Meng and Z. Wei, *RSC Adv.*, 2013, **3**, 23957–23962.
14 L. Kou, T. Huang, B. Zheng, Y. Han, X. Zhao, K. Gopalsamy, H. Sun and C. Gao, *Nat. Commun.*, 2014, **5**, 3754.
15 L. Kou, Z. Liu, T. Huang, B. Zheng, Z. Tian, Z. Deng and C. Gao, *Nanoscale*, 2015, **7**, 4080–4087.
16 B. Zheng, T. Huang, L. Kou, X. Zhao, K. Gopalsamy and C. Gao, *J. Mater. Chem. A*, 2014, **2**, 9736–9743.
17 X. Zhao, B. Zheng, T. Huang and C. Gao, *Nanoscale*, 2015, **7**, 9399–9404.
18 Z. Xu and C. Gao, *ACS Nano*, 2011, **5**, 2908–2915.
19 Z. Xu and C. Gao, *Nat. Commun.*, 2011, **2**, 571.
20 Z. Liu, Z. Li, Z. Xu, Z. Xia, X. Hu, L. Kou, L. Peng, Y. Wei and C. Gao, *Chem. Mater.*, 2014, **26**, 6786–6795.
21 Z. Li, Z. Liu, H. Sun and C. Gao, *Chem. Rev.*, 2015, **115**, 7046–7117.
22 Z. Xu and C. Gao, *Acc. Chem. Res.*, 2014, **47**, 1267–1276.
23 Z. Xu and C. Gao, *Mater. Today*, 2015, **18**, 480–492.
24 X. Hu, Z. Xu and C. Gao, *Sci. Rep.*, 2012, **2**, 767.
25 L. Kou and C. Gao, *Nanoscale*, 2013, **5**, 4370–4378.
26 Z. Liu, Z. Xu, X. Hu and C. Gao, *Macromolecules*, 2013, **46**, 6931–6941.
27 X. Zhao, Z. Xu, B. Zheng and C. Gao, *Sci. Rep.*, 2013, **3**, 3164.
28 X. Ding, Y. Zhao, C. Hu, Y. Hu, Z. Dong, N. Chen, Z. Zhang and L. Qu, *J. Mater. Chem. A*, 2014, **2**, 12355–12360.
29 J. Zhang, P. Chen, B. H. L. Oh and M. B. Chan-Park, *Nanoscale*, 2013, **5**, 9860–9866.
30 H. Kashani, L. Chen, Y. Ito, J. Han, A. Hirata and M. Chen, *Nano Energy*, 2016, **19**, 391–400.
31 A. Davies, P. Audette, B. Farrow, F. Hassan, Z. Chen, J.-Y. Choi and A. Yu, *J. Phys. Chem. C*, 2011, **115**, 17612–17620.
32 Y. Zhao, J. Liu, Y. Hu, H. Cheng, C. Hu, C. Jiang, L. Jiang, A. Cao and L. Qu, *Adv. Mater.*, 2013, **25**, 591–595.
33 Y. Liu, H. Wang, J. Zhou, L. Bian, E. Zhu, J. Hai, J. Tang and W. Tang, *Electrochim. Acta*, 2013, **112**, 44–52.
34 X. Wang, C. Yang and P. Liu, *Synth. Met.*, 2012, **162**, 2349–2354.
35 X. Hu, Z. Xu, Z. Liu and C. Gao, *Sci. Rep.*, 2013, **3**, 2374.
36 X. Zhao, Z. Xu, B. Zheng and C. Gao, *Sci. Rep.*, 2013, **3**, 3164.
37 H. Li, Y. Tao, X. Zheng, J. Luo, F. Kang, H.-M. Cheng and Q.-H. Yang, *Energy Environ. Sci.*, 2016, **9**, 3135–3142.
38 P. Huang, C. Lethien, S. Pinaud, K. Brousse, R. Laloo, V. Turq, M. Respaud, A. Demortière, B. Daffos, P. L. Taberna, B. Chaudret, Y. Gogotsi and P. Simon, *Science*, 2016, **351**, 691–695.
39 C. Zhang, W. Lv, Y. Tao and Q.-H. Yang, *Energy Environ. Sci.*, 2015, **8**, 1390–1403.
40 Y. Xu, Y. Tao, X. Zheng, H. Ma, J. Luo, F. Kang and Q.-H. Yang, *Adv. Mater.*, 2015, **27**, 8082–8087.
41 M. Ghidiu, M. R. Lukatskaya, M.-Q. Zhao, Y. Gogotsi and M. W. Barsoum, *Nature*, 2014, **516**, 78–81.
42 X. Yang, C. Cheng, Y. Wang, L. Qiu and D. Li, *Science*, 2013, **341**, 534–537.
43 Y. Tao, X. Xie, W. Lv, D.-M. Tang, D. Kong, Z. Huang, H. Nishihara, T. Ishii, B. Li, D. Golberg, F. Kang, T. Kyotani and Q.-H. Yang, *Sci. Rep.*, 2013, **3**, 2975.
44 L. F. Warren and D. P. Anderson, *J. Electrochem. Soc.*, 1987, **134**, 101–105.
45 I. K. Moon, J. Lee, R. S. Ruoff and H. Lee, *Nat. Commun.*, 2010, **1**, 73.
46 X. Feng, N. Chen, Y. Zhang, Z. Yan, X. Liu, Y. Ma, Q. Shen, L. Wang and W. Huang, *J. Mater. Chem. A*, 2014, **2**, 9178–9184.
47 X. Feng, Z. Yan, N. Chen, Y. Zhang, X. Liu, Y. Ma, X. Yang and W. Hou, *New J. Chem.*, 2013, **37**, 2203–2209.
48 X. Feng, N. Chen, J. Zhou, Y. Li, Z. Huang, L. Zhang, Y. Ma, L. Wang and X. Yan, *New J. Chem.*, 2015, **39**, 2261–2268.
49 D.-W. Wang, F. Li, J. Zhao, W. Ren, Z.-G. Chen, J. Tan, Z.-S. Wu, I. Gentle, G. Q. Lu and H.-M. Cheng, *ACS Nano*, 2009, **3**, 1745–1752.
50 Y. Sun and G. Shi, *J. Polym. Sci., Part B: Polym. Phys.*, 2013, **51**, 231–253.
51 X.-L. Wu, T. Wen, H.-L. Guo, S. Yang, X. Wang and A.-W. Xu, *ACS Nano*, 2013, **7**, 3589–3597.
52 Z.-S. Wu, G. Zhou, L.-C. Yin, W. Ren, F. Li and H.-M. Cheng, *Nano Energy*, 2012, **1**, 107–131.
53 P. Simon and Y. Gogotsi, *Nat. Mater.*, 2008, **7**, 845–854.
54 B. Hsia, J. Marschewski, S. Wang, J. B. In, C. Carraro, D. Poulikakos, C. P. Grigoropoulos and R. Maboudian, *Nanotechnology*, 2014, **25**, 055401.
55 T. Y. Kim, H. W. Lee, M. Stoller, D. R. Dreyer, C. W. Bielawski, R. S. Ruoff and K. S. Suh, *ACS Nano*, 2011, **5**, 436–442.
56 Q. Cheng, J. Tang, J. Ma, H. Zhang, N. Shinya and L.-C. Qin, *Phys. Chem. Chem. Phys.*, 2011, **13**, 17615–17624.
57 M. Beidaghi and C. Wang, *Adv. Funct. Mater.*, 2012, **22**, 4501–4510.
58 L. L. Zhang, S. Zhao, X. N. Tian and X. S. Zhao, *Langmuir*, 2010, **26**, 17624–17628.
59 B. Saswata, K. Nam Hoon, K. Tapas, L. Kin-tak and L. Joong Hee, *Nanotechnology*, 2011, **22**, 295202.
60 J. Zhang, Y. Yu, L. Liu and Y. Wu, *Nanoscale*, 2013, **5**, 3052–3057.

61 S. Ye and J. Feng, *ACS Appl. Mater. Interfaces*, 2014, **6**, 9671–9679.
62 H. Zhou, G. Han, Y. Xiao, Y. Chang and H.-J. Zhai, *J. Power Sources*, 2014, **263**, 259–267.
63 Y. Huang, M. Zhu, Y. Huang, H. Li, Z. Pei, Q. Xue, Z. Liao, Z. Wang and C. Zhi, *J. Mater. Chem. A*, 2016, **4**, 4580–4586.
64 H. Ge, G. Qi, E.-T. Kang and K. G. Neoh, *Polymer*, 1994, **35**, 504–508.

Published on 12 April 2017. Downloaded by Zhejiang University on 21/06/2017 06:44:38.

This journal is © The Royal Society of Chemistry 2017